# A facile method for promoting activities of ordered mesoporous silica-anchored Rh–P complex catalysts in 1-octene hydroformylation†

**Wei Zhou and Dehua He***

***Received 12th January 2009, Accepted 30th April 2009***
***First published as an Advance Article on the web 14th May 2009***
**DOI: 10.1039/b900591a**

This work deals with the promotion of immobilized Rh catalyst activities in olefin hydroformylation by lengthening the alkyl spacers and choosing an active Rh precursor. The flexibility of long chain alkyls was used to free the motion of the anchored Rh complex in confining porous spaces so as to increase the substrate activation efficiency. $RhCl(CO)(PPh_3)_2$ was anchored to mesoporous silicas SBA-15 and MCM-41 through *n*-alkyl (carbon number $n = 1$, 3, 5, 8, 11) as spacer. The catalysts were characterized by X-ray powder diffraction (XRD), isothermal $N_2$ sorption analysis and inductive coupling plasma-atomic emission spectroscopy (ICP-AES). The multi-step-assembly of the complex into surface-organic modified mesoporous silica was monitored and evidenced by infrared spectroscopy (IR). The prepared Rh-immobilized catalysts were applied in 1-octene hydroformylation to nonyl aldehydes. Rh leaching in the reaction solutions was determined by ICP-MS, which was found to be satisfyingly low along with successful catalyst cycles. With the increase of the alkyl spacer length, the specific activity (shown as turnover number, TON) and stability of the immobilized catalyst were both increased. The catalyst prepared by the longest alkyl spacer ($n = 11$, $C_{11}$) revealed activity comparable to the homogeneous counterpart and resistance to the by-product poisoning. $RhCl(CO)(PPh_3)_2$-supported catalysts were also prepared by impregnating $RhCl(CO)(PPh_3)_2$ into SBA-15 and MCM-41 without the presence of diphenylphosphinoalkyl, the prepared catalysts showed a sharp activity decrease within only two catalyst cycles, owing to the significant active species leaching.



## 1. Introduction

Zeolite chemists take for granted that the invention[1] of ordered mesoporous silica (hereafter OMS) is consequent to the requirement of processing large molecules, either as active compositions or reactants. These materials are synthesized by self-assembled surfactants as template,[2,3] which can be removed by calcination or solvent-extraction. With hexagonal symmetry and honeycomb-like pore channels, MCM-41[4] and SBA-15[5,6] are apparently the most widely studied OMS referring to applications such as separation, chemical sensing[7] and catalysis.[8] OMSs are promising supports for hosting catalytic species varying from monometallic complexes[9,10] to nanoparticles,[11,12] benefiting from their high specific surface area, high adsorption capacity, easy surface modification and certain hydro/solvothermal stabilities. In addition, the confining effects[13] of porous materials enhance the intermolecular interactions inside the nanospaces, which is exactly the origin of the concept of a *molecular sieve.* Consequently, the ordered mesopores have advantages over amorphous silica, nano $SiO_2$ and active carbon, since they offer a uniform confining function and activity sites thereby form.[14]

Currently, as the largest industrial homogeneous process, hydroformylation of olefins[15] with syngas (equimolar CO and $H_2$) produces aldehydes with one more carbon than the initially employed olefin. The products, including alcohols by further hydrogenation of aldehydes, are widely employed in the production of detergents, solvents, softeners and plasticizers with great market profits. Hydroformylation can be catalyzed by Rh–P complexes, for example oil-soluble $RhCl(PPh_3)_3$, $RhCl(CO)(PPh_3)_2$ or water-soluble $RhCl(CO)(TPPTS)_2$ (TPPTS = triphenylphosphine-3,3′,3″-trisulfonic acid trisodium salt). The reaction goes under mild conditions with a great turnover number (TON) of substrate. Heterogenization of the Rh complex to the support has potential industrially, since it aims at easy catalyst separation and recycling, atom-economy and low metal loss, and in this aspect OMS is a good support candidate. Immobilization of Rh complexes to MCM-41, MCM-48 and SBA-15 has been previously reported.[16–18] Although the immobilized catalysts are easily recyclable, the catalytic application of the OMS-anchored Rh complex encounters two main problems. First, the leaching of active species is sometimes serious over successful catalyst cycles, since the complex is not stably immobilized. A general solution is to apply better ligands for stable coordination. Li *et al.*[16] recently

*Innovative Catalysis Program, Key Lab of Organoelectronics & Molecular Engineering of Ministry of Education, Department of Chemistry, Tsinghua University, Beijing, 100084, China. E-mail: hedeh@mail.tsinghua.edu.cn; Fax: +8610 6277 3346; Tel: +8610 6277 3346*

† Electronic supplementary information (ESI) available: GC-MS analysis of the 18-carbon $\alpha,\beta$-unsaturated aldehyde produced by the dehydration of the aldol consendation adduct of nonyl aldehydes in the 1-octene hydroformylation catalyzed by $S–C_3–PPh_2–[RhCl(CO)(PPh_3)_2]$ (3rd catalyst cycle) in the present study. See DOI: 10.1039/b900591a

 

reported a dendritic SBA-15 supported Wilkinson's catalyst for the styrene hydroformylation and Rh leaching was minimized. The other significant problem is the decrease of catalyst activity compared to homogeneous counterparts, which is related to mass transfer. More effective ligands can be then employed[19] to promote the heterogenized catalyst activities. This can be achieved by corresponding homogeneous catalyst study advances. Peng *et al.*[18] employed two triphenylphosphine analogs as additional ligands to MCM-41 or MCM-48 anchored Rh–N complex catalysts. The immobilized catalysts showed activity and linear product selectivity comparable to corresponding homogeneous counterparts in the 1-hexene hydroformylation.

To chemically bond the catalytic organometallic complex to the inorganic support, some organic medium is required as spacer. Hence, organic functionalization[20,21] of the OMS to produce a hybrid material is generally performed before further possible modification. Previous researches have been focusing on altering the ligand, either the ligand connected to spacer or the ligand additionally added. In our recent work,[22] $RhCl_3$ as precursor was anchored to SBA-15 modified with diphenylphosphinoalkyl ($-(CH_2)_nPPh_2$, $n = 1, 3, 5, 8, 11$). The catalysts were employed in the 1-octene hydroformylation and it was found that the TON of 1-octene was increased with the lengthening of the alkyl spacer. The catalyst prepared with the longest alkyl spacer ($C_{11}$) showed comparable activity to the homogeneous precursor $RhCl_3$. The selectivity however was higher, probably because the by-products were restricted in the pores. Rh leaching in the reaction solution was found to be satisfyingly low, owing to the stable complexity of the phenyl phosphine ligand.[23] However, these immobilized catalysts SBA-15–$C_n$–$PPh_2$–[$RhCl_3$] showed lower activity than the homogeneous $RhCl(CO)(PPh_3)_2$, probably owing to the less efficient precursor that was used. It was found[22,24] by choosing a more active Rh precursor that the heterogenized catalyst activity was promoted. In the present work, $RhCl(CO)(PPh_3)_2$, the famous catalyst for hydroformylation developed by UCC, will be employed as Rh precursor to prepare OMS-anchored Rh–P complex catalysts. The OMS support involves the structurally similar SBA-15 and MCM-41. 1-Octene hydroformylation to nonyl aldehydes will be still applied as a probe reaction. We will show that the alkyl spacer is a significant function in promoting OMS-anchored Rh–P complex activities in the 1-octene hydroformylation. For a comparison, $RhCl(CO)(PPh_3)_2$-supported catalysts (without the diphenylphosphinoalkyl-modification of the support) will be also prepared and applied.

## 2. Experimental

### 2.1 Preparation of the catalysts

**2.1.1 Synthesis of SBA-15 and MCM-41 (OMS).** Preparation of the OMS-immobilized Rh catalysts is shown in Scheme 1.

**SBA-15** was synthesized in a three-necked flask.[6,22] Tri-block copolymer P123 ($PEO_{20}PPO_{70}PEO_{20}$, $M_n = 5800$, Aldrich) was dissolved in HCl (2 mol $L^{-1}$). Tetraethyl orthosilicate (TEOS, Acrös) was added dropwise. The mixture was stirred for 20 h under 308 K. The flask was then sealed and kept under 353 K for 24 h. Molar ratio of the initial gel was 0.02 P123 : 40 $H_2O$ : 4.78 HCl : 1.00 TEOS. The resulting solid was recovered and washed until the filtrate was neutral. The as-synthesized SBA-15 was calcined at 773 K for 6 h with a temperature-ramp of 1 K $min^{-1}$.

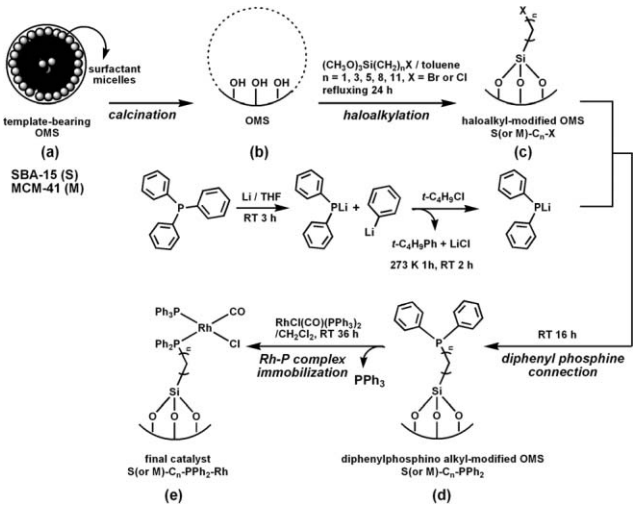


**Scheme 1** Preparation of Rh-immobilized catalysts.

**MCM-41** was synthesized according to literature methods.[4,12,24] In a typical synthesis, ammonia (aq) and cetyltrimethylammonium bromide (CTABr) were dissolved in deionized water under vigorous stirring. TEOS was then added dropwise. After stirring for 2 h, a gel with a molar composition of 0.12 CTABr : 112 $H_2O$ : 8 $NH_4OH$ : 1.00 TEOS was obtained, transferred into a Teflon-lined autoclave and then heated at 383 K for 72 h. The solid product was recovered by filtration and washed with deionized water until the filtrate was neutral. The as-synthesized material was calcined at 823 K for 6 h in air with a temperature-programmed rate of 1 K $min^{-1}$.

**2.1.2 Surface modification: haloalkylation by silane.** 1.00 g OMS was suspended in toluene (A.R.) and 3.0 mL trimethoxysilane $X(CH_2)_nSi(OCH_3)_3$ was added (silanes with alkyl spacer $n =$ 1, 3, 11 were purchased from Gelest; silanes with spacer $n = 5$ and 8 were synthesized according to literature methods,[22,25,26] X = Br in the case of $n = 11$, for the rest X = Cl). The above mixture was refluxed for 24 h. The resulting solid was recovered by filtration and washed with dichloromethane in a Soxhlet's extractor for 12 h to remove the organic species physisorbed. Haloalkyl-modified OMSs are denoted as "S(or M)–$C_n$–X". S indicates SBA-15 and M indicates MCM-41. Alkyl carbon number $n = 1, 3, 5, 8, 11$. X is the haloatom (Cl or Br).

**2.1.3 Diphenylphosphine ligand connection.** The connection of diphenyl phophine ligands ($-PPh_2$) was carried out under Schlenk operation conditions. THF (A.R.) was in advance refluxed with sodium under nitrogen for dehydration and deoxidation. 20.8 g triphenyl phosphine (Fluka) was dissolved in 200 mL THF. 1.1 g lithium turnings (A.R., Sinopharm Chemical Reagent Co., Ltd) were then added. The mixture was stirred at room temperature and in dry nitrogen atmosphere for 3 h. After removing the surplus metal, 9.0 mL *tert*-butyl chloride (C.P., Sinopharm Chemical Reagent Co., Ltd) was added at 273 K to decompose the phenyllithium. The electromagnetic stirrer was held at 273 K for 1 h and then at room temperature for 2 h. S(or M)–$C_n$–X was afterwards mixed with the red

lithium diphenylphosphide solution and the continuous stirring was held for 16 h at room temperature. The resulting solid was recovered and washed with dichloromethane in nitrogen atmosphere for 12 h. Diphenylphosphinoalkyl-modified OMS is denoted as S(or M)–$C_n$–$PPh_2$.

**2.1.4 Immobilization of $RhCl(CO)(PPh_3)_2$ complex.** The immobilization of $RhCl(CO)(PPh_3)_2$ (Strem) was finished by mixing S(or M)–$C_n$–$PPh_2$ in dichloromethane with the rhodium precursor (10 wt%), which was stirred at room temperature and in nitrogen atmosphere for 36 h.[24,27,28] The final solid catalyst was recovered and ultrasonic-washed to remove uncoordinated ions.[12] The catalyst is denoted as S(or M)–$C_n$–$PPh_2$–Rh.

Seven OMS-anchored Rh–P complex catalysts were prepared, including S–$C_n$–$PPh_2$–Rh ($n = 1, 3, 5, 8, 11$) and M–$C_n$–$PPh_2$–Rh ($n = 3, 5$).

**2.1.5 Preparation of $RhCl(CO)(PPh_3)_2$-supported catalysts.** For comparison, $RhCl(CO)(PPh_3)_2$-supported catalysts were prepared by the impregnation method. Support OMS (SBA-15 or MCM-41) was mixed with $RhCl(CO)(PPh_3)_2$ (10 wt%) in dichloromethane. The mixture was stirred at room temperature and in nitrogen atmosphere for 36 h. The catalyst was recovered and washed with dichloromethane until the filtrate was colorless. $RhCl(CO)(PPh_3)_2$-supported catalyst is denoted as $RhCl(CO)(PPh_3)_2$/S or $RhCl(CO)(PPh_3)_2$/M.

### 2.2 Characterization of catalysts

Powder X-ray diffraction (XRD) data at low angles were collected on a Rigaku D/max-RB diffractometer at a scan solution of 2° $min^{-1}$ with CuK$\alpha$ radiation ($\lambda = 0.1542$ nm). XRD characterization was powered at 40 kV and 100 mA. Fourier-transform infrared spectrometry (FT-IR) in the 4000 $cm^{-1}$ to 450 $cm^{-1}$ range was operated on a Perkin SpectrumOne spectrometer by KBr wafers (1 wt% of sample). Isothermal nitrogen sorption analysis at 77 K was performed on a Micromeritics ASAP 2010 analysis system; the BET (Brunauer–Emmett–Teller) and BJH (Barrett–Joyner–Halenda) methods were applied for the specific surface area and pore size distribution calculations, respectively. Rh contents of the immobilized and supported catalysts were obtained by an IRIS Intrepid II Inductive Coupling Plasma-Atomic Emission Spectroscopy (ICP-AES) spectrometer. Leached Rh contents in reaction solutions were analyzed by an X series In 20000CPS/ppb (1.5%RSD) ICP-MS spectrometer. 2 mL reaction solution was calcined at 573 K to evaporate all liquids. 0.5 mL $H_2SO_4$ (98%) was added to the residue and heated to eliminate organic residues. Then, 1.0 mL $HNO_3$ (63%) was added. The resulting acidic liquid mixture was then diluted to 25 mL for ICP-MS analysis. Determination of the by-product was finished by a Shimadzu GCMS-QP2010S system.

**2.3 1-Octene hydroformylation.** 1-Octene hydroformylation was carried out as follows. 5.0 mL 1-octene (Acrös, 99%) was mixed with 15.0 mL toluene (A.R.) in a 100 mL autoclave and the catalyst was added. The autoclave was then firmly sealed and syngas (equimolar $H_2$ and CO) was injected at a temperature lower than 278 K to replace the air inside the autoclave (3×). The autoclave was heated to 393 K and the syngas was injected to 5.0 MPa. The electromagnetic stirring was started and lasted for 2.5 h. At the end of the reaction, the autoclave was cooled to lower than 278 K and the pressure was released. 1.0 mL isopropyl alcohol (A.R.) was added as internal standard. The resulting mixture was analyzed by a GC-HP4890 equipped with a HP-5 capillary column (0.25 mm × 30 m). In the catalyst recycling experiments, the separated catalysts were above all washed by toluene under ultrasonic washing[12] to remove residual substances.

## 3. Results and discussion

### 3.1 Catalyst characterization results

**3.1.1 X-ray diffraction (XRD).** Fig. 1 shows the XRD patterns of catalysts S–$C_n$–$PPh_2$–Rh ((A), $n = 1, 3, 5, 8, 11$) and M–$C_n$–$PPh_2$–Rh ((B), $n = 3, 5$). All the XRD patterns revealed ordered hexagonal symmetry with a well-resolved (100) reflection.[1,5] The preparative procedure of the catalysts did not ruin the support structure, revealing the good solvothermal stabilities of SBA-15 and MCM-41. The (100) reflection is associated with the unit cell parameter $a_0$ of the hexagonal symmetry by the equation,[4]

$$a_0 = \frac{2}{\sqrt{3}} d_{100} \quad (1)$$

where $a_0$ equals the pore size plus one wall thickness and $d_{100}$ is the interplanar crystal spacing. By the Bragg's equation it is known,

$$n\lambda = 2d_{100} \times \sin\theta \quad (2)$$

where $\lambda$ is the radiation wavelength. By eqn (1) and (2), the (100) reflection located at lower 2Theta for larger pores. In Fig. 1, SBA-15-anchored catalysts (A) gave the (100) reflection at *ca.*

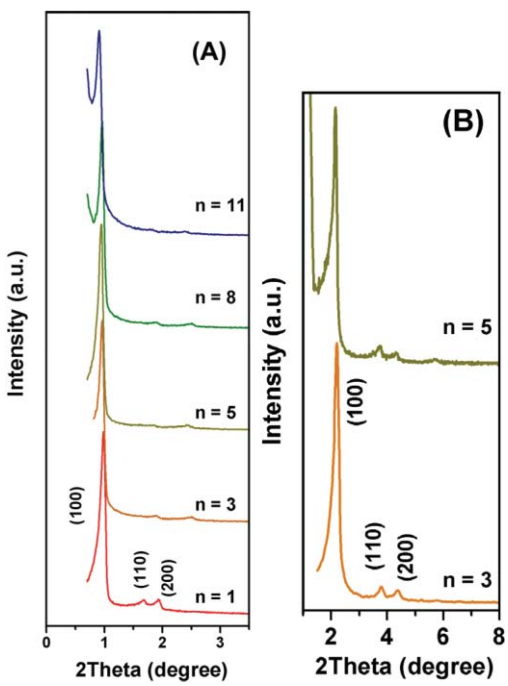


**Fig. 1** XRD patterns of (A) S–$C_n$–$PPh_2$–Rh and (B) M–$C_n$–$PPh_2$–Rh.

 

2Theta = 1.00°, and MCM-41-anchored catalysts (B) show the reflection at *ca.* 2Theta = 2.30°.

**3.1.2 Infrared spectroscopy (IR).** To clarify the immobilized catalyst structure formed inside the OMS pores still remains difficult. However, as it has been developed in our experiments,[22,24] IR spectroscopy has been shown to be powerful for monitoring the multi-step-assembly of the complex into the OMS if critical IR absorptions are carefully assigned.[29] Since the organic modified OMSs were washed during the preparation of catalyst, the physisorption was beyond consideration. Two examples are presented in Fig. 2 with quite similar regularities and conclusions. Please refer to Scheme 1 for sample correspondence.

When $RhCl(CO)(PPh_3)_2$ was anchored to SBA-15 through spacer $C_3$ (Fig. 2(A)), $\nu_{as}$(C–H) at 2933 $cm^{-1}$, $\nu_s$(C–H) at 2878 $cm^{-1}$, and $\delta$(C–H) at 1457, 1375, 1350 and 1296 $cm^{-1}$ in P123-bearing SBA-15 (a) vanished after calcination (b), indicating the successful removal of the polymer template. These peaks reappeared after chloropropyl-modification (c) by 3-chloropropyltrimethoxyl silane. The absorption at 955 $cm^{-1}$ (b) was significantly weakened after chloropropylation (from (b) to (c)), revealing that the amount of modifiable silanols[30] decreased owing to silane modification. The successful chloropropyl-modification was also reflected in the observation of $\nu$(C–Si) at 696 $cm^{-1}$ and $\nu$(C–Cl) at 647 $cm^{-1}$ (c). $\nu$(C–Si) was preserved after connection with $-PPh_2$ ligands (d) and the immobilization of $RhCl(CO)(PPh_3)_2$ (e), indicating that the grafted silanes were not lost. $\nu$(C–Cl) disappeared after the C–P bond formation (d), showing $\nu$(C–P) at 748 $cm^{-1}$. S–$C_3$–$PPh_2$ (d) showed an intense and broad aromatic skeleton stretching at 1508 $cm^{-1}$ owing to the conjugation of phosphorous p elections with π electrons of phenyls. Aromatic $\delta$(C–H) was observed at 866 $cm^{-1}$. A weak absorption at 3073 $cm^{-1}$ arose due to the overtone contributed by $\nu$(Ar C=C) and $\nu$(Ar C–H) of single-substituted benzene. $\nu$(Ar C=C) was weakened after Rh complex immobilization (from (d) to (e)), probably because the cation withdrew electrons from the ligands. This also showed the interaction of the $-(CH_2)_3PPh_2$ ligand with Rh, implying the successful immobilization of the complex. $\nu$(C=O) was observed at 1979 $cm^{-1}$ (see insert). The stretching of the Si–O–Si bond[31] in the saturated range of 1290 to 996 $cm^{-1}$ and $\delta$(Si–O–Si) at 467 $cm^{-1}$ were observed through the multi-step modification, indicating that the SBA-15 framework was not affected, which is in accordance with the XRD characterization.

Similar regularities were found if IR was performed to monitor the immobilization of $RhCl(CO)(PPh_3)_2$ to diphenylphosphinopentyl-modified MCM-41 (Fig. 2(B)). CTABr-bearing MCM-41 (a) showed intense $\nu_{as}$(C–H) at 2922 $cm^{-1}$, $\nu_s$(C–H) at 2852 $cm^{-1}$ and long chain alkyl rocking at neighboring 1488, 1481, 1473, and 1465 $cm^{-1}$. $\nu(N^+–H)$ was observed at 1397 $cm^{-1}$; $\delta(N^+–H)$ was observed at 838, 720, and 697 $cm^{-1}$ (a). These absorptions disappeared after calcination with the terminal silanol stretching found at 3747 $cm^{-1}$ ((b) and insert). The signal characteristic of the modifiable degree of MCM-41 showed at 966 $cm^{-1}$ (b), and it was weakened after silane grafting (from (b) to (c)). After the grafting of silane (c), $\nu_{as}$(C–H) at 2958 $cm^{-1}$, $\nu_s$(C–H) at 2851 $cm^{-1}$, $\nu$(C–Si) at 693 $cm^{-1}$, and $\nu$(C–Cl) at 647 $cm^{-1}$ were observed. The connection of $-PPh_2$ ligands (d) produced $\nu$(C–P) at 741 $cm^{-1}$ and a broad $\nu$(Ar C=C) band at 1508 $cm^{-1}$. The overtone shown by $\nu$(Ar C=C) and $\nu$(Ar C–H) of single-substituted benzene was similarly found at *ca.* 3070 $cm^{-1}$. $\nu$(Si–O–Si) stretching appeared in the 1250 to 1000 $cm^{-1}$ range and was preserved. The corresponding IR absorption of organic species seems stronger

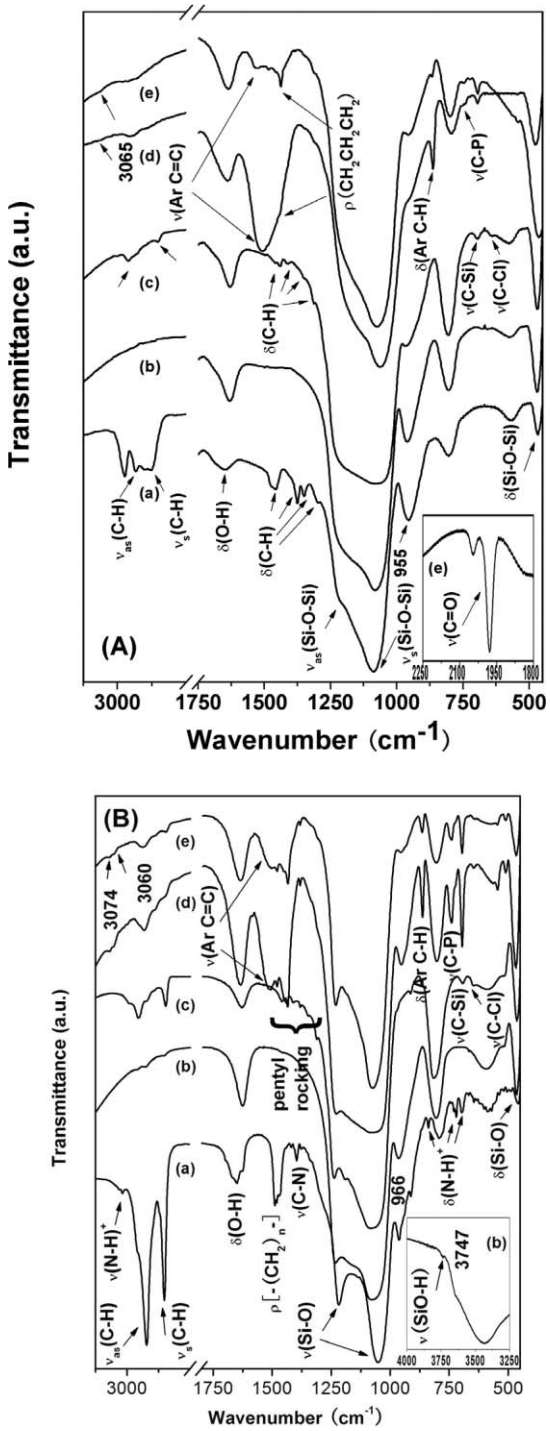


**Fig. 2** FT-IR spectra of (A): P123-bearing SBA-15 (a), calcined SBA-15 (b), S–$C_3$–Cl (c), S–$C_3$–$PPh_2$ (d), S–$C_3$–Rh (e). Insert: an enlarged area of the S–$C_3$–Rh catalyst showing the carbonyl stretching. (B): CTABr-bearing MCM-41 (a), calcined MCM-41 (b), M–$C_5$–Cl (c), M–$C_5$–$PPh_2$ (d), M–$C_5$–Rh. Insert: an enlarged area of calcined MCM-41 showing the stretching of the terminal silanol.

than that of the SBA-15-based materials, since MCM-41 has a thinner $SiO_2$ framework.

**3.1.3 $N_2$ sorption analysis.** Fig. 3 shows the isotherms of parent SBA-15 and S–$C_n$–$PPh_2$–Rh catalysts (A) and the corresponding pore size distribution of the samples (B). All the isotherms revealed to be type IV according to the IUPAC classification,[32] characteristic of typical ordered mesoporous materials. S–$C_n$–$PPh_2$–Rh catalysts gave type H1 hysteresis loop, revealing the uniform pore size distribution and highly ordered mesostructure, which was consistent with the XRD characterization. Some textual properties of the catalysts are summarized in Table 1. The immobilization of Rh complex into mesoporous SBA-15 decreased the BET specific surface area of the material, probably because the inner surface had been tailored with polar species and thus the adsorption of nitrogen molecules was more difficult. With the increase of alkyl spacer length, the hysteresis occurred at lower $P/P_0$, indicating the decrease of pore size.

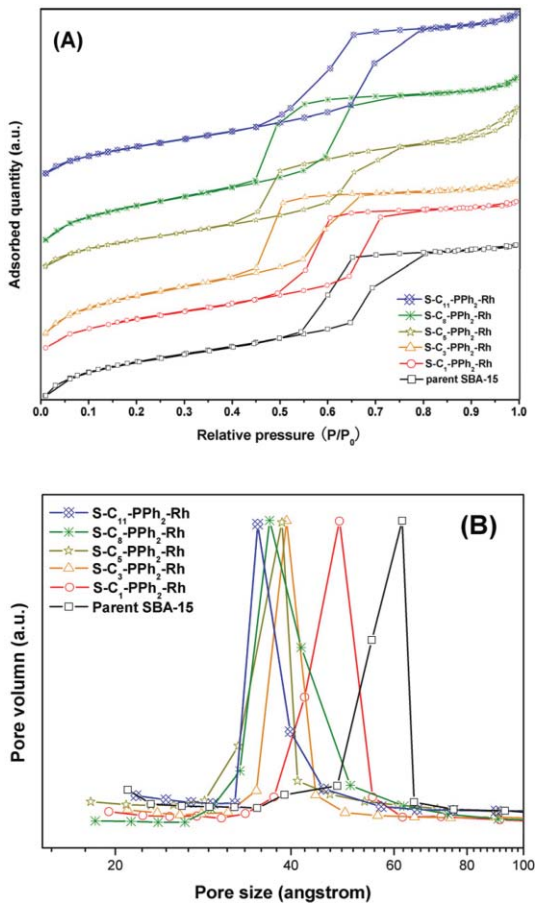


**Fig. 3** (A) Isotherms of parent SBA-15 and S–$C_n$–$PPh_2$–Rh catalysts and (B) $D_{BJH}$ pore size distribution of SBA-15 and S–$C_n$–$PPh_2$–Rh catalysts.

On the other hand, the assemble of organometallic species also increased the bulky density of the materials. Noticeably, although the $D_{BJH}$ somewhat decreased with the increase of spacer length (Table 1), their differences were not consistent with theoretical calculation with C–C bond length, probably owing to the flexibility of the alkyl spacer.[18]

**Table 1** Textual properties and Rh contents of the catalysts

| | $S_{BET}$[a]/$m^2\ g^{-1}$ | $D_{BJH}$[a]/nm | $V_P$[a]/$cm^3\ g^{-1}$ | Rh[b](wt%) |
|---|---|---|---|---|
| SBA-15 | 673 | 6.2 | 0.75 | — |
| S–$C_1$–$PPh_2$–Rh | 440 | 4.8 | 0.53 | 0.22 |
| S–$C_3$–$PPh_2$–Rh | 375 | 3.9 | 0.35 | 0.35 |
| S–$C_5$–$PPh_2$–Rh | 355 | 3.8 | 0.38 | 0.32 |
| S–$C_8$–$PPh_2$–Rh | 385 | 3.6 | 0.39 | 0.29 |
| S–$C_{11}$–$PPh_2$–Rh | 429 | 3.5 | 0.45 | 0.28 |
| MCM-41[c] | 755 | 2.75 | 0.52 | — |
| M–$C_3$–$PPh_2$–Rh[c] | 693 | 2.52 | 0.43 | 1.50 |
| M–$C_5$–$PPh_2$–Rh | 642 | 2.28 | 0.38 | 1.20 |
| $RhCl(CO)(PPh_3)_2$/S | — | — | — | 0.38 |
| $RhCl(CO)(PPh_3)_2$/M | — | — | — | 0.50 |

[a] $S_{BET}$: BET specific surface area; $D_{BJH}$: BJH primary pore diameter; $V_P$: single point total pore volume. [b] Immobilized-Rh contents were determined by ICP-AES analysis. [c] Data from ref. 24.

MCM-41 and M–$C_n$–$PPh_2$–Rh catalysts (Fig. 4) also revealed type IV isotherms with H1 hysteresis loop.[24] However, the hysteresis loops revealed by MCM-41-anchored catalysts were smaller and the isotherms were more likely approaching langmuir-type (Fig. 4(A)). This is probably because the pore size

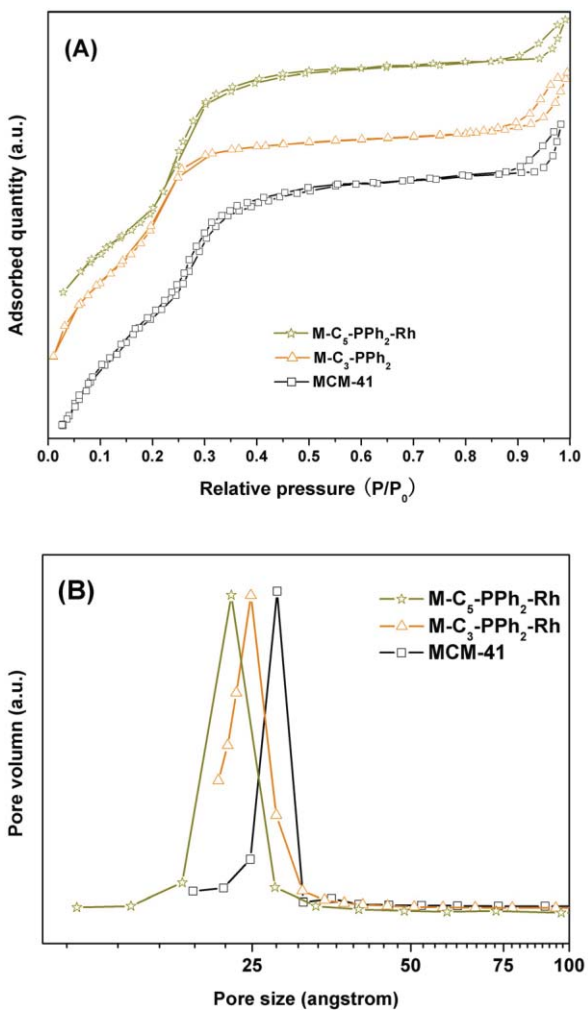


**Fig. 4** (A) Isotherms of parent MCM-41 and M–$C_n$–$PPh_2$–Rh catalysts and (B) $D_{BJH}$ pore size distribution of MCM-41 and S–$C_n$–$PPh_2$–Rh catalysts. Data of M–$C_3$–$PPh_2$–Rh are from ref. 24.

 

of MCM-41-anchored catalysts are just a little bigger than 2 nm (Table 1). Textual properties of MCM-41 and M–$C_n$–$PPh_2$–Rh are summarized in Table 1. M–$C_n$–$PPh_2$–Rh catalysts had higher $S_{BET}$ than S–$C_n$–$PPh_2$–Rh catalysts because of the thinner $SiO_2$ framework.

### 3.2 1-Octene hydroformylation results

**3.2.1 Reaction operation conditions and specific activity definition.** 1-Octene hydroformylation conditions were the same as our previous work[22,24] so that a comparison could be made. Initial syngas pressure ($CO/H_2$) was 5.0 MPa; reaction temperature was 393 K, and reaction time was 2.5 h. 1-Octene hydroformylation was also performed by corresponding homogeneous counterparts under the same reaction conditions. Turnover number (TON) is adopted for disclosing the specific catalyst activity and efficiency, which is defined as,

$$\text{TON} = \text{molar}\,\frac{\text{converted 1-octene}}{\text{immobilized Rh}} \quad (3)$$

**3.2.2 Catalyst turnover capacity.** The results of the 1-octene hydroformylation catalyzed by S(or M)–$C_n$–$PPh_2$–Rh catalysts are shown in Fig. 5(B) and (C). Previous work[22] is also quoted for comparison (Fig. 5(A)). Fig. 5(A), (B) and (C) are plotted with the same scale of TON (vertical axis on the left) and selectivity of nonyl aldehydes (vertical axis on the right). (A) and (B) show the results from Rh-immobilized catalysts with the same support (SBA-15) but different Rh precursors, while (B) and (C) show the results from the catalysts with the same precursor ($RhCl(CO)(PPh_3)_2$) but different OMSs as support. Two purple dot lines are respectively plotted in (A) and (B), showing the results catalyzed by corresponding homogeneous catalysts under the same reaction conditions.

According to Fig. 5, 1-octene TON was increased with the increasing length of alkyl spacer. Catalysts prepared with the shortest spacer ($C_1$, the red lines in (A) and (B)) revealed the lowest 1-octene TON. Catalysts prepared with the longest alkyl spacer ($C_{11}$, the royal blue lines in (A) and (B)) revealed an activity comparable to the homogeneous counterpart (the purple dot lines in (A) and (B)). Obviously, the catalyst prepared with $RhCl(CO)(PPh_3)_2$ as precursor (B) revealed a much higher activity than the corresponding analogue prepared with $RhCl_3$ as precursor (A), indicating that the catalyst activity could be further promoted by choosing a more active precursor, similar to the strategy of synthesizing more efficient ligands to promote the immobilized catalyst activity.[18] The high turnover capacity revealed by the OMS-anchored Rh catalyst through the longer alkyl as spacer might result from the flexibility of the alkyl. A longer alkyl spacer brings the anchored catalyst far from the solid surface and the motion of the anchored catalyst is thus relatively free. According to (B) and (C), corresponding S–$C_n$–$PPh_2$–Rh and M–$C_n$–$PPh_2$–Rh with the same alkyl spacer ($C_3$ and $C_5$, respectively) revealed a similar 1-octene TON. This indicates that the OMS-anchored Rh complex catalyst activity depends greatly on the spacer length, as long as inner mass transfer is eliminated.

In contrast, $RhCl(CO)(PPh_3)_2$-supported catalysts (black dash–dot lines showing 1-octene TON in Fig. 5(B) and (C)) showed a very quick activity loss when the catalysts were recycled. Both $RhCl(CO)(PPh_3)_2$/S and $RhCl(CO)(PPh_3)_2$/M revealed a sharp activity decrease within only two catalyst cycles. This is because without the diphenylphosphinoalkyl that covalently bonds the complex and the support, the Rh species leaches significantly during catalyst cycles.[18] Noticeably, fresh $RhCl(CO)(PPh_3)_2$-supported catalyst revealed an activity as high as the homogeneous $RhCl(CO)(PPh_3)_2$-catalyzed process.

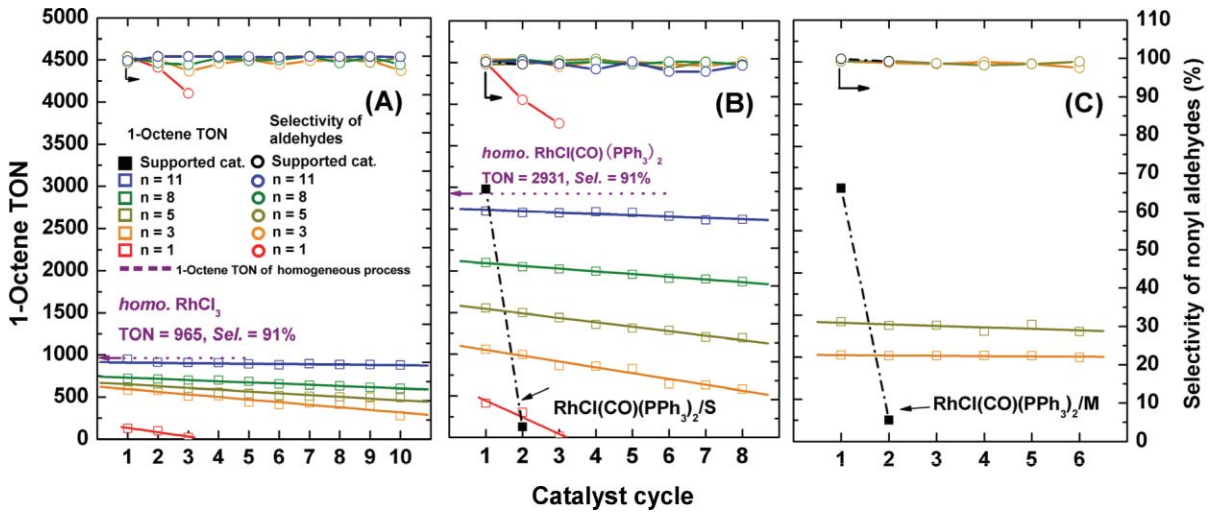


**Fig. 5** 1-Octene hydroformylation results over the catalysts. (A) SBA-15–$C_n$–$PPh_2$–[$RhCl_3$], by using $RhCl_3$ as precursor, data from ref. 22; (B) SBA-15–$C_n$–$PPh_2$–[$RhCl(CO)(PPh_3)_2$] *viz.* S–$C_n$–$PPh_2$–Rh defined in the present work, by using $RhCl(CO)(PPh_3)_2$ as precursor; (C) M–$C_n$–$PPh_2$–Rh, by using MCM-41 as support and $RhCl(CO)(PPh_3)_2$ as precursor, M–$C_3$–$PPh_2$–Rh data from ref. 24. (□) 1-Octene TON, (○) selectivity of nonyl aldehydes. A specific spacer is given a specific color, (red) $n = 1$, (orange) $n = 3$, (dark yellow) $n = 5$, (olive) $n = 8$, (royal blue) $n = 11$. Homogeneous processes are in purple dot lines, $RhCl(CO)(PPh_3)_2$-supported catalysts results in black dash–dot lines. Reaction temperature 393 K, initial syngas pressure 5.0 MPa, reaction time 2.5 h. Initial Rh/1-octene ratio ($\times 10^{-4}$): 1.2 (S–$C_1$–$PPh_2$–Rh), 1.9 (S–$C_3$–$PPh_2$–Rh), 1.7 (S–$C_5$–$PPh_2$–Rh), 1.6 (S–$C_8$–$PPh_2$–Rh), 1.5 (S–$C_{11}$–$PPh_2$–Rh), 2.6 (homogeneous $RhCl(CO)(PPh_3)_2$), 1.8 ($RhCl(CO)(PPh_3)_2$/S), 4.5 (M–$C_3$–$PPh_2$–Rh), 3.3 (M–$C_5$–$PPh_2$–Rh), 2.3 ($RhCl(CO)(PPh_3)_2$/M).

**Table 2** Ratio of linear and branched nonyl aldehydes shown by Rh-immobilized and $RhCl(CO)(PPh_3)_2$-supported catalysts along with catalyst cycles

| | Ratio of linear/branched nonyl aldehydes (*n*/*i*) | | | | | | | |
|---|---|---|---|---|---|---|---|---|
| | Catalyst cycle | | | | | | | |
| Catalyst | 1 | 2 | 3 | 4 | 5 | 6 | 7 | 8 |
| S–$C_1$–$PPh_2$–Rh | 1.8 | 1.6 | 1.6 | — | — | — | — | — |
| S–$C_3$–$PPh_2$–Rh | 1.6 | 1.7 | 1.8 | 1.7 | 1.4 | 1.9 | 1.7 | 1.5 |
| S–$C_5$–$PPh_2$–Rh | 1.6 | 1.6 | 1.5 | 1.7 | 1.6 | 1.8 | 1.4 | 1.5 |
| S–$C_8$–$PPh_2$–Rh | 1.6 | 1.4 | 1.3 | 1.5 | 1.3 | 1.3 | 1.4 | 1.3 |
| S–$C_{11}$–$PPh_2$–Rh | 1.3 | 1.4 | 1.3 | 1.2 | 1.5 | 1.4 | 1.5 | 1.3 |
| M–$C_3$–$PPh_2$–Rh[a] | 1.5 | 1.4 | 1.6 | 1.5 | 1.7 | 1.8 | — | — |
| M–$C_5$–$PPh_2$–Rh | 1.6 | 1.5 | 1.7 | 1.8 | 1.4 | 1.5 | — | — |
| $RhCl(CO)(PPh_3)_2$/S | 1.6 | 1.8 | — | — | — | — | — | — |
| $RhCl(CO)(PPh_3)_2$/M | 0.6 | 1.5 | — | — | — | — | — | — |

[a] Data from ref. 24.

This is because supported Rh species leached into the reaction solution and thus a homogeneous process took place. After the first cycle of $RhCl(CO)(PPh_3)_2$/M, 82% of the supported Rh had been detected to have leached into the liquid.

**3.2.3 *n*/*i* ratio of nonyl aldehydes.** Table 2 shows the ratio of linear and branched products of nonyl aldehydes along with catalyst cycles. The *n*/*i* ratio varied in the range of 1.0 to 2.0 along with the catalyst cycles, which seemed lower since hydroformylation is accompanied by isomerization.[33] It appears that catalysts prepared with longer alkyl spacers revealed a lower *n*/*i* ratio. These catalysts prepared with $RhCl(CO)(PPh_3)_2$ as precursor showed higher selectivity towards linear products than the catalyst analogs[22] prepared with $RhCl_3$ as precursor, as a result of abundant triphenyl phosphine ligands.

**3.2.4 Catalyst stability and Rh leaching.** In Fig. 5, the OMS-anchored Rh catalysts could be employed along with several cycles in 1-octene hydroformylation, but the catalysts revealed quite different stabilities. The catalysts prepared with methyl ($C_1$) as spacer (red lines in Fig. 5(A) and (B)) revealed an obvious activity decrease within three catalyst cycles. On the contrary, the catalysts prepared with longer spacers show relative stability. The catalysts prepared with the longest alkyl spacer ($C_{11}$, royal blue lines in (A) and (B)) could be successfully employed along with several cycles with no obvious activity decrease observed. With the increasing length of alkyl spacer, the stability of the prepared catalysts was increased as the slope of the plotted TON line becomes lower (Fig. 5(A) and (B)). The stability of M–$C_n$–$PPh_2$–Rh catalysts (Fig. 5(C)) will be discussed later.

In order to investigate whether Rh leaching is the reason for the catalyst activity decrease, reaction solutions were analyzed for leached Rh content. Table 3 summarizes the total Rh leaching percentage from the sum of catalyst cycles for every immobilized catalyst. According to the data presented, the Rh leaching is satisfyingly low, comparing with related work.[34] MCM-41-based catalysts revealed even lower active species leaching, probably resulting from the higher specific area (see Table 1). Both the good coordination capacity of the phosphine ligand[23] and the confining effect originating from the larger surface area of OMS-anchored Rh–P catalyst contribute to the lower Rh leaching.

**Table 3** Rh leaching from S(or M)–$C_n$–$PPh_2$–Rh catalysts[a]

| Catalyst | Catalyst cycle times | Total Rh leaching (%) | Average Rh leaching per cat. cycle (%) |
|---|---|---|---|
| S–$C_1$–$PPh_2$–[$RhCl_3$][b] | 3 | 1.1 | 0.37 |
| S–$C_3$–$PPh_2$–[$RhCl_3$][b] | 10 | 2.3 | 0.23 |
| S–$C_5$–$PPh_2$–[$RhCl_3$][b] | 10 | 2.5 | 0.25 |
| S–$C_8$–$PPh_2$–[$RhCl_3$][b] | 10 | 1.4 | 0.14 |
| S–$C_{11}$–$PPh_2$–[$RhCl_3$][b] | 10 | 1.3 | 0.13 |
| S–$C_1$–$PPh_2$–Rh | 3 | 4.0 | 1.30 |
| S–$C_3$–$PPh_2$–Rh | 8 | 3.8 | 0.48 |
| S–$C_5$–$PPh_2$–Rh | 8 | 3.3 | 0.41 |
| S–$C_8$–$PPh_2$–Rh | 8 | 3.0 | 0.38 |
| S–$C_{11}$–$PPh_2$–Rh | 8 | 2.9 | 0.36 |
| M–$C_3$–$PPh_2$–Rh[c] | 6 | 0.29 | 0.05 |
| M–$C_5$–$PPh_2$–Rh | 6 | 0.22 | 0.04 |

[a] Determined by ICP-MS. [b] Prepared with $RhCl_3$ as precursor, data from ref. 22. [c] Data from ref. 24, S = SBA-15, M = MCM-41. Rh = using $RhCl(CO)(PPh_3)_2$ as precursor.

Additional work was carried out by pre-treating the fresh S–$C_3$–$PPh_2$–Rh catalyst (which showed a moderate catalyst activity decrease along with catalyst cycles among the analogues) with toluene at 393 K and 5.0 MPa syngas pressure for 2.5 h (exactly the hydroformylation conditions). Following the hydroformylation operations in section 2.3 and reaction conditions described in section 3.2.1, the catalyst was stirred in fresh toluene. The mother liquid was collected, to which 1-octene was added. The mixed liquids were allowed to carry out the hydroformylation under the same reaction conditions, and the result was a 1-octene TON = 53. The treated catalyst was again treated with toluene and the collected solvent was mixed with 1-octene. Hydroformylation of the mixed liquids then resulted in a 1-octene TON of 8. The two-time-treated catalyst S–$C_3$–$PPh_2$–Rh was employed in 1-octene hydroformylation, and the substrate TON was 566, with a 97% activity compared to the fresh catalyst without pre-treating with toluene. By pre-treating the catalyst, the active species immobilized to the external surface[18] of SBA-15 were most likely to be removed. Although washing assisted by an ultra-sonic device can remove the uncoordinated



 

species when synthesizing the catalyst,[12] it appears that some active species will only leach under the reaction conditions.

Both the determination of the leached Rh in the reaction solution and the pre-treating fresh catalyst experiment indicate the good stability of the Rh–P complex. Thus, Rh leaching won't account for the catalyst activity decrease along with catalyst cycles observed in Fig. 5(A) and (B).

**3.2.5 Surface properties of recycled catalysts.** Infrared spectroscopic analysis has been performed on recycled catalysts, as is shown in Fig. 6. The IR spectra of recycled catalysts were quite different from those of the fresh catalysts. The stretching vibration of saturated C–H, aromatic C=C stretching, C–P as well as C–Si stretchings were greatly enhanced. Aromatic C–H stretching can be observed as the shoulder peak of alkyl C–H stretching. The rocking of the long chain $–CH_2–$, as a fingerprint of polymeric alkane,[35] was clearly observed as a series of neighboring peaks in the range of 1500 to 1300 $cm^{-1}$. A new peak was observed at *ca.* 1700 $cm^{-1}$, which could be assigned to the $\nu$(C=O) in the $\alpha,\beta$-unsaturated species.[22,29,36] The stretching vibrations were significantly enhanced, which implies that a compound with conjunction structure exists in the recycled catalysts.

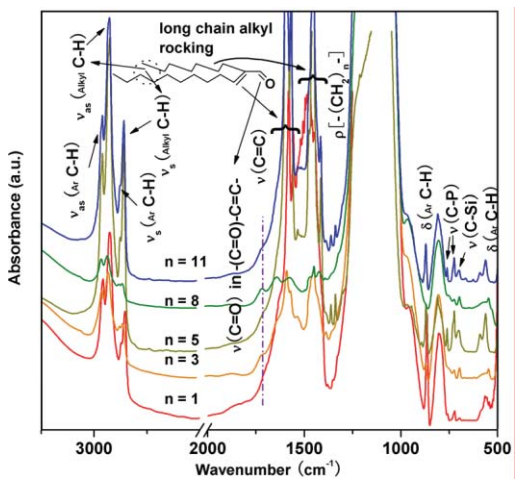


**Fig. 6** FT-IR spectra of recycled S–$C_n$–$PPh_2$–Rh catalysts.

The aldol condensation of the aldehyde product has been regarded as the side reaction of olefin hydroformylation.[15] Owing to the stability by conjunction, the aldol condensation adduct of the aldehyde will dehydrate, forming an acyclic $\alpha,\beta$-unsaturated compound. On the basis of the literature[15] and the IR spectra, we assume that an 18-carbon $\alpha,\beta$-unsaturated aldehyde, which is the dehydrated product of the aldol condensation adduct of nonyl aldehyde, was produced and coordinated with Rh (Scheme 2) owing to the confining effect and high surface area of porous materials. This product has been determined by the GC-MS analysis of the reaction solution (see ESI).† The phosphorous p electrons, phenyl π electrons, π electrons from C=C and C=O in the $\alpha,\beta$-unsaturated aldehyde, and the rhodium d electrons together lead to a strong conjunction and thus stabilizes the coordination of the $\alpha,\beta$-unsaturated aldehyde with Rh. The conjunction enhanced all the stretching IR vibrations as mentioned in Fig. 6. Shown in Fig. 7, the

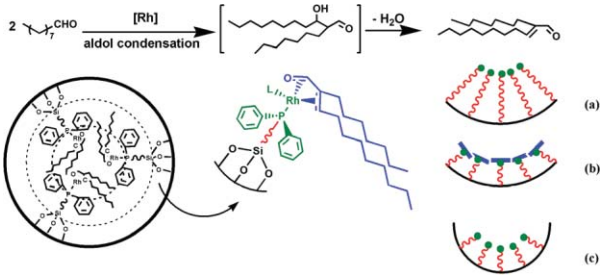


**Scheme 2** The dehydrated product of the aldol condensation adduct coordinates with Rh so as to poison it. (a) Longer spacers on larger pores with lower surface curvature; (b) shorter spacers on larger pores; (c) shorter spacers on smaller pores with higher curvature.

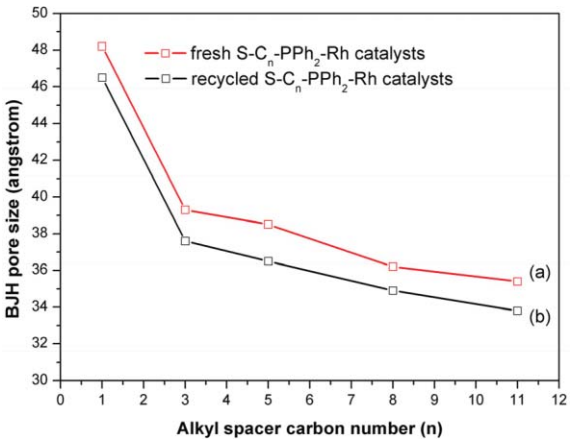


**Fig. 7** BJH pore size of S–$C_n$–$PPh_2$–Rh catalysts (a) fresh and (b) recycled.

BJH pore size of the recycled catalysts was slightly decreased compared to the corresponding fresh catalyst, which evidences that the unsaturated aldehyde exists inside the pores.

The stably coordinated $\alpha,\beta$-unsaturated aldehyde was difficult to release during the catalytic process, and thus the catalysts were irreversibly poisoned. The poisoning of catalysts in hydroformylations has been also found in homogeneous processes.[37,38] When a longer spacer is employed, the pore size of the catalyst is smaller. The terminal active sites (Scheme 2(a)) can stretch into a smaller central circle, which disfavors the linear aldehyde coordination owing to the steric hindrance. Catalysts with the spacer $C_{11}$ (royal blue lines in (A) and (B), Fig. 5) showed no obvious activity decrease during the catalyst recycles. However, when a shorter spacer was employed (Scheme 2(b)), the terminal active sites stretched into a larger circle, not far from the support surface. The immobilized Rh–P complex maintains a relatively longer distance with each other, which favors the by-product coordination and such complex is inert towards hydroformylation. When MCM-41 was employed as support, the catalysts had smaller pores than the SBA-15-anchored Rh–P complex. Smaller pores had higher surface curvature, which allowed shorter spacers to stretch into smaller circles and to approach each other near (Scheme 2(c)), providing similar resistance to the by-product coordination. This might be the reason why the M–$C_n$–$PPh_2$–Rh ($n$ = 3, 5) catalysts showed a relatively more stable capacity of substrate turnover than the corresponding S–$C_n$–$PPh_2$–Rh ($n$ = 3, 5) analogues (Fig. 5, compare (B)

and (C)), as no obvious activity decrease was observed when M–$C_n$–$PPh_2$–Rh catalyst was recycled (Fig. 5(C)).

On the other hand, the by-product was confined in the pores of the catalysts so it was in lower concentration in the reaction solution. Consequently, the solid catalysts showed higher selectivity than homogeneous processes (Fig. 5(A) and (B)).

## 4. Conclusions

The present work is a continuing study[22] on alkyl spacer effects of ordered mesoporous silica-anchored Rh–P complex catalysts in olefin hydroformylation. In conclusion, the present work introduces a facile method to promote ordered mesoporous silica-anchored Rh–P complex catalyst activities in olefin hydroformylation by simply lengthening the alkyl spacers that covalently connect the support and the anchored complex and choosing a more efficient Rh precursor. The length of the alkyl spacer has a drastic effect on the specific activity (shown as turnover number of substrate, TON) of the immobilized catalysts. The catalyst prepared with the longest alkyl spacer ($C_{11}$) revealed a specific activity comparable to the homogeneous counterpart. The immobilized catalysts reveal a remarkable low Rh leaching along with successful catalyst cycles. The dehydrated product of the aldol condensation adduct of nonyl aldehydes might be the reason for the catalyst activity decrease. A longer spacer on SBA-15 helps the Rh-immobilized catalysts to resist the by-product poisoning coordination owing to steric hindrance. Similarly, when MCM-41 is employed as support, it has a higher surface curvature; shorter spacers can provide the steric hindrance function to resist by-product coordination.



## Acknowledgements

This work is financially supported by the National Natural Science Foundation of China (No. 20673064), Specialized Research Fund for the Doctoral Program of Higher Education of Ministry of Education of China (2007003108) and Fund for Analysis of Tsinghua University. Wei Zhou would like to thank Mr Qingwei Zheng for his help in GC-MS analysis of the by-product.

## Notes and references

1 C. T. Kresge, M. E. Leonowicz, W. J. Roth, J. C. Vartuli and J. S. Beck, *Nature*, 1992, **359**, 710.
2 G. J. de, A. A. Soler-Illia, C. Sanchez, B. Lebeau and J. Patarin, *Chem. Rev.*, 2002, **102**, 4093.
3 Y. Wan and D. Zhao, *Chem. Rev.*, 2007, **107**, 2821.
4 J. S. Beck, J. C. Vartuli, W. J. Roth, M. E. Leonowicz, C. T. Kresge, K. T. Schmitt, C. T. W. Chu, D. H. Olson, E. W. Sheppard, S. B. McCullen, J. B. Higgins and J. L. Schlenker, *J. Am. Chem. Soc.*, 1992, **114**, 10834.
5 D. Zhao, J. Feng, Q. Huo, N. Melosh, G. H. Fredrickson, B. F. Chmelka and G. D. Stucky, *Science*, 1998, **279**, 548.
6 D. Zhao, Q. Huo, J. Feng, B. F. Chmelka and G. D. Stucky, *J. Am. Chem. Soc.*, 1998, **120**, 6024.
7 S. Tao, G. Li and H. Zhu, *J. Mater. Chem.*, 2006, **16**, 4521.
8 A. Taguchi and F. Schüth, *Microporous Mesoporous Mater.*, 2005, **77**, 1.
9 D. E. De Vos, M. Dams, B. F. Sels and P. A. Jacobs, *Chem. Rev.*, 2002, **102**, 3615.
10 A. Corma and H. Garcia, *Adv. Synth. Catal.*, 2006, **348**, 1391.
11 X.-Y. Hao, W. Zhou, J.-W. Wang, Y.-Q. Zhang and S. Liu, *Chem. Lett.*, 2005, **34**, 1000.
12 X.-Y. Hao, Y.-Q. Zhang, J.-W. Wang, W. Zhou, C. Zhang and S. Liu, *Microporous Mesoporous Mater.*, 2005, **88**, 38.
13 K. Ariga, A. Vinu, Q. Ji, O. Ohmori, J. P. Hill, S. Acharya, J. Koike and S. Shiratori, *Angew. Chem., Int. Ed.*, 2008, **47**, 7254 and literatures therein cited.
14 L. Mercier and T. J. Pinnavaia, *Adv. Mater.*, 1997, **9**, 500.
15 G. van Koten and P. W. N. M. van Leeuwen, in *Catalysis: an Integrated Approach*, ed. R. A. van Santen, P. W. N. M. van Leeuwen, J. A. Moulijn and B. A. Averill, Elsevier, Amsterdam, 2nd edn, 1999, ch. 6.
16 P. Li and S. Kawi, *Catal. Today*, 2008, **231**, 61.
17 L. Huang, Y. He and S. Kawi, *J. Mol. Catal. A: Chem.*, 2004, **213**, 241.
18 Q. Peng, Y. Yang and Y. Yuan, *J. Mol. Catal. A: Chem.*, 2004, **219**, 175.
19 A. J. Sandee, L. A. van der Veen, J. N. H. Reek, P. C. J. Kamer, M. Lutz, A. L. Spek and P. W. N. M. van Leeuwen, *Angew. Chem., Int. Ed.*, 1999, **38**, 3231.
20 C. Zhang, W. Zhou and S. Liu, *J. Phys. Chem. B*, 2005, **109**, 24319.
21 F. Hoffmann, M. Cornelius, J. Morell and M. Fröba, *Angew. Chem., Int. Ed.*, 2006, **45**, 3216.
22 W. Zhou and D. He, *Chem. Commun.*, 2008, 5839.
23 M. T. Honaker, B. J. Sandefur, J. L. Hargett, A. L. McDaniel and R. N. Salvatore, *Tetrahedron Lett.*, 2003, **44**, 8373.
24 W. Zhou and D. He, *Catal. Lett.*, 2009, **127**, 437.
25 C. S. Marvel and W. E. Garrison, Jr, *J. Am. Chem. Soc.*, 1959, **81**, 4737.
26 R. A. Benkeser, S. D. Smith and J. L. Noe, *J. Org. Chem.*, 1968, **33**, 597.
27 S.-G. Shyu, S.-W. Cheng and D.-L. Tzou, *Chem. Commun.*, 1999, 2337.
28 J. Kramer, E. Nöllen, W. Buijs, W. L. Driessen and J. Reedijk, *React. Funct. Polym.*, 2003, **57**, 1.
29 J. Dean, in *Analytical Chemistry Handbook*, McGraw-Hill Book Co., Singapore, 1995, Section 6.
30 B. Tian, X. Liu, C. Yu, F. Gao, W. Luo, S. Xie, B. Tu and D. Zhao, *Chem. Commun.*, 2002, 1186.
31 L. Zhao, S. Wang, Y. Wu, Q. Hou, Y. Wang and S. Jiang, *J. Phys. Chem. C*, 2007, **111**, 18387.
32 K. S. W. Sing, D. H. Everett, R. A. W. Haul, L. Moscou, R. A. Pierotti, J. Rouquérol and T. Siemieniewska, *Pure Appl. Chem.*, 1985, **57**, 603.
33 A. C. J. Koeken, M. C. A. van Vliet, L. J. P. van den Broeke, B.-J. Deelman and J. T. F. Keurentjes, *Adv. Synth. Catal.*, 2008, **350**, 179.
34 B. Tan, J. Jiang, Y. Wang, L. Wei, D. Chen and Z. Lin, *Appl. Organomet. Chem.*, 2008, **22**, 620.
35 N.-C. Chia and R. Mendelsob, *J. Phys. Chem.*, 1992, **96**, 10534.
36 IR spectrum of acrolein is available from Aldrich website, see http://www.sigmaaldrich.com/catalog/search/ProductDetail/ALDRICH/110221.
37 G. Liu and M. Gardland, *Organometallics*, 1999, **18**, 3459.
38 Y. Liu, D. He, C. Li, T. Wang, J. Liu and Q. Zhu, *Chin. J. Mol. Catal.*, 2000, **14**, 337.

 